Spectrum of Engineering Sciences
ISSN (e) 3007-3138 **(p)** 3007-312X **Volume 3, Issue 6, 2025**

NUMERICAL HEAT TRANSFER ON JET IMPINGEMENT COOLING OF CHIPS WITH SQUARE HOLES

Attiq Ur Rehman[1], Muhammad Shahid Farooq[2], Khawar Abbas[3], Hassaan Ahmad[4], Dong Yang[*5]

*[1,2,*5]State Key Laboratory of Multiphase Flow in Power Engineering, Xi'an Jiao Tong University, Xi'an 710049, China*
[4]State Key Lab of Aerospace Power System and Plasma Technology, Xi'an Jiao Tong University, Xi'an 710049, China, School of Mechanical Engineering, Xi'an Jiao Tong University, Xi'an 710049, China
[3]School of Management, Xi'an Jiao Tong University

[*5]dyang@mail.xjtu.edu.cn

DOI: https://doi.org/10.5281/zenodo.15771490

Keywords
Numerical simulations, Enhance Heat Transfer, Convection, Nusselt Number, Pressure drop

Article History
Received on 21 May 2025
Accepted on 21 June 2025
Published on 30 June 2025

Corresponding Author: * Dong Yang

Abstract

This work presents a three dimensional (3-D) incompressible flow numerical simulation in order to investigate the natural convection heat transfer and laminar flow through jet square holes, Enhance Heat transfer between solid material and fluid was considered and under investigate in the numerical analysis. This heat transfer and fluid flow phenomena numerically analyze assume continuity equation, momentum equation and energy equation and adopt thermal equilibrium model by using commercial CFD software ANSYS Fluent software 19.0. Boundary condition in this numerical analysis generalized through SIMPLE algorithm scheme. Three-dimensional incompressible flow simulation of heat transfer and laminar flow represents the results of Nusselt number (Nu), pressure drop (ΔP). A numerical solution using governing equation, continuity equation, momentum equation and energy equation of partial differential equation is obtained using SIMPLE algorithm scheme and for pressure, energy and momentum used second order & second order upwind scheme for gradient used Least Square cell based. Titanium electrode used as heat source Fluid as HFE7000 is used as coolant flow impinge on the titanium electrode (heat source). Initialization the problem used Hybrid Initialization solution method. The result obtain are discussed in term of Nusselt number, pressure drop with different jet arrangement pattern at 45 (L/s) volume flow rate.

INTRODUCTION

The Jet impingement can be applied to many fields, including the impinging of high temperature/pressure air flow during rocket launch, the cooling of blades in steam turbines, the drying of food, and the cooling of electronic devices. Specifically, in terms with single-phase cooling for electronic devices, jet cooling can achieve excellent thermal performance. Fluid flow and convection heat transfer have been widely investigated experimentally and numerically for many years due to the many important applications [1]. Heat transfer through jet impingement holes has a great scope in chemical, mechanical, aerospace, medical, geothermal reservoirs, drying of porous solids, thermal insulation, enhanced oil recovery, packed-bed catalytic reactors, cooling of nuclear reactors and underground energy transport [2] biological engineering, materials sciences & many more fields [3], [4].

Recent advances in electronic system, heat exchangers, chemical reactors, etc. have led to dramatic increases in heat flux. A numerical study is performed to analyze the steady state natural convection fluid flow and heat transfer through a plate as medium that is partially inserted into to 3D channel to enhanced the heat transfer and laminar flow. To analyzed this phenomenon used different equation and mathematical model to investigate the heat transfer and fluid flow, this Numerical Study Investigated through Numerical Simulation using ANSYS FLUENT 19.0 Analyze the effects of velocity, hole diameter, pressure drop and Nusselt Number on heat transfer rate and laminar flow. The Investigation were carried out on rectangular Titanium electrode is deposited on Pyrex substrate by CVD method as heat source. Governing equation, momentum and energy equation are used to enhanced heat transfer and laminar flow simulation. The fluid flow used as HFE7000 that set different parameter of fluid density 1481kgm^{-3}, viscosity 0.000565 kg m^{-1} s^{-1}, specific heat of HEF7000 1300 Jkg^{-1} K^{-1} and thermal conductivity of HEF7000 was 0.07906 wm^{-1} K^{-1} details of physical data of fluid and solid phase given in

Table 1. Heat transfer investigate on the different Nusselt Number (Nu) and change in Pressure (ΔP) calculate fluid flow velocity of 45mL/min. In this numerical study we consider the steady state three-dimensional fluid flow and Heat Transfer of viscous fluid (Laminar flow) of 3D channel. However, the 3D numerical stimulation scheme is highly efficient in computations. The solution is obtained numerically using mathematical model and governing equation of fluid flow and heat transfer and the effects of Nusselt number (Nu) and pressure drop (ΔP). The most common Dimensionless Parameters that are used to characterized the heat transfer data are Nu, Prandlt number (Pr), Grashof numbers (Gr), Reynolds number (Re), etc. Heat transfer continues to be a field of major interest to engineers, scientific researchers, manufacturers. It is transfer of heat from one body to another body due to temperature difference. Heat transfer takes place whenever there is a temperature gradient within a system or whenever two systems at different temperatures are brought into contact. Generally, heat transfer takes place in three different modes: conduction, convection and radiation.

Convection heat transfer and fluid flow with porous medium occur in power stations of many engineering applications where cooling or heating is required such as cooling turbine blades, cooling electronic equipment and combustion systems. Suma et.al. [5] described that convection heat transfer takes place between a surface and a moving fluid, when there is temperature gradient exists. Convection is effect of fluid motion and conduction. The rate of heat transfer is depending upon temperature difference as well as fluid motion. The heat transferred through the surface from one side to other, can be written as in terms of the Newton's law of Cooling [6], [7]. Convection heat transfer process is express by Newton's law of cooling as;

$$Q = hA\,(T_s - T_f) \qquad (1)$$

Where Q is rate of heat transfer, h is convective heat transfer coefficient, A is area through which heat is transfer, T_s is surface temperature and T_f temperature of fluid. The overall model which is used in simulation is shown below in Figure 1 below.

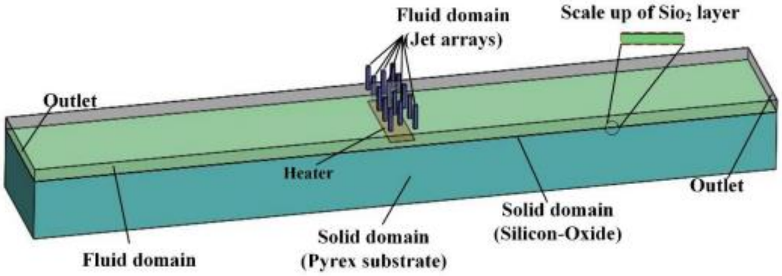

Figure 1: Synoptic Simulation Model

Table 1 Physical Properties

Fluid	Densitykg/m^3	Specific heat J/(kg·K	Thermal conductivityW/(m·K)	Viscositykg/(m·s)
HFE 7000	1481	1300	0.07906	0.000565
SiO2	2200	1000	0.6	
Pyrex	2230	750	1.143	

Mathematical Analysis

Governing Equation

The Computational model (governing equation) for the Heat Transfer and Laminar Flow from HEF 7000 based on Nu pressure drop at velocity of 45ml/min are described in equ. 2 below. The General Governing Equation for fluid flow and Heat Transfer is.

$$\partial(\rho\phi)/\partial t + \nabla\cdot(\rho\phi U) = \nabla\cdot(\Gamma * \nabla\phi) + S\phi \qquad (2)$$

Where
ρ = density
ϕ = scalar quantity
U = velocity vector
Γ = diffusion coefficient
$S\phi$ = source term

Continuity Equation

Two-Dimensional differential form of the continuity equation is:

$$\partial u/\partial x + \partial v/\partial y = 0 \qquad (3)$$

$$\partial \rho /\partial t + \nabla . (\rho u) = 0 \qquad (4)$$

Finite Volume Method (FVM)

Finite Volume Method has been first selection of the mostly commercial computational fluid dynamics (CFD) software such as ANSYS FUENT. In present work the numerical finite volume (FVM) approach is utilized for discretization the all-partial differential equations into algebraic form. Finite volume method physical domain of model is discretized into finite set of control volume (CV) and all variable are positioned ate the centroid of each volume. The Finite Volume Method (FVM) is a technique for interpretation and estimation of partial differential equation (PDE's) in the format of an algebraic equation. Finite Volume Method (FVM) is one of the highly multipurpose discretization method which implement in computational fluid dynamics (CFD). The dependent variables value is conserved in Finite Volume Method (FVM) at the "center of element or centroid volume" in other words all fluid flow properties volume flow rate, pressure, temperature and density to be solved in center of control volume (CV).

k-ε Turbulence Model

The k-ε turbulence model are extensively applied in commercial CFD software to simulate the mean flow characteristics for turbulent flow condition. It is also called two equation model that provides a general explanation of turbulence flow by means of two transport equation. The k-ε turbulence model is suitable for complex shear flows including moderate swirl, vortices and boundary layer separations and accurately predict the flow spreading rate for both planer & circular jets.

Numerical Simulation & Boundary Condition

The present study using SIMPLE algorithm scheme and thermal equilibrium model for the jet. The impingement, numerical data obtained governing equation, energy and momentum equation for each nodes and element are used to get value of Nusselt number, pressure drop, PN, static temperature & pressure and velocity contour, then plot graphically representation of these results. Simulation were done by ANSYS Fluent 19.0. The mesh is mainly composed of quadrilateral grid elements, and a few triangular grid elements are also applied to improve the quality of mesh. This study proved that the numerical results obtained in the current investigation are grid independent. The Energy equation solved by the Finite Volume Method, during the process of iteration the convergence time is adjusted by the changing the relaxation factor of the Energy equation.

In addition, the convergence of the numerical solution is judged only by the monitoring the residual temperature level. In this numerical study, all calculations are based on the double Persian and processing option was kept parallel. Final relaxation factor of the energy equation is 1 and for momentum 0.7 and the solution is finally regarded as convergent when the residual is less than 10−12 and heat flow rate on the both sides reaches equilibrium.

Geometric Symmetry, two planes of symmetry Mesh

The element size of $5 \times 10^{-5} m$, was used in the flow domain, and the element size near the heat source and jets was reduced to $1.25 \times 10^{-5} m$, using body of influence sizing method as shown in **Figure 2**. Rest of the solid domain were left with the default element sizes, since there is no need of small elements to capture the turbulence. The mesh for pattern 1 contained 198072 Nodes, and678497 elements.

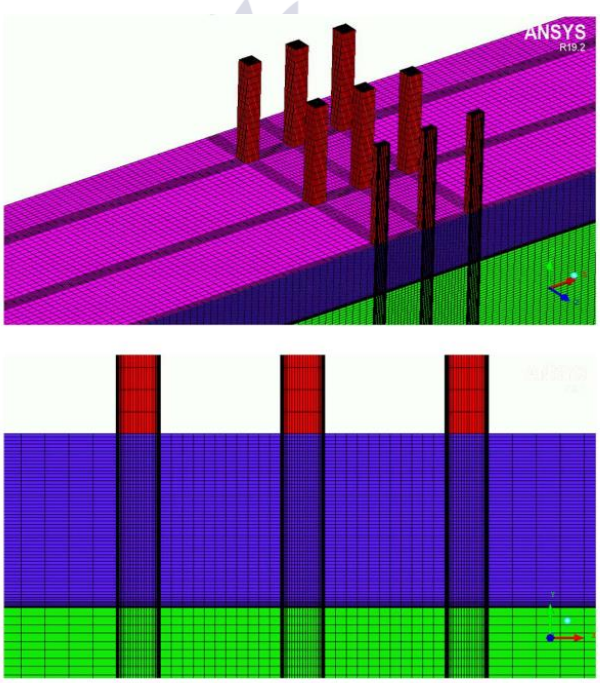

Figure 2: Showing Symmetry Mesh of planes

Mass flow rate was calculated by using the density of HFE7000, and ¼ times of the calculated mass flow rate was defined at the inlet, since the domain was reduced to ¼th by applying the geometric symmetries.

Table 2 show the boundary conditions outputs and other related informations.

Table 2 boundary Conditions Outputs

Inlet	Mass flow inlet	2.78e-4 kg/s	10 ℃
Outlet	Pressure Outlet		
Heat source	Heat Flux	8.0e+5 W/m^2	
Internal walls	Symmetryboundary conditions		
All interfaces	Thermally Coupled		
All walls	No slip		

K-epsilon turbulence model was used with enhanced wall treatment, and solution was converged to residual error of the order of 10^{-3}, and 10^{-6} for energy equation. Y+ < 2.5, at the jets, and surface of the heat source.

Results and discussions

The results and discussion section is structured to provide a comprehensive analysis of the thermal and fluid dynamics performance of the three patterns, focusing on key parameters such as Nusselt number, pressure distribution, temperature contours, and velocity profiles. For each pattern, the Nusselt number distributions are examined to evaluate the efficiency of convective heat transfer, highlighting regions of enhanced or diminished thermal performance. Pressure distributions are then analyzed to understand the flow resistance and stability associated with each design, while temperature contours reveal thermal gradients and uniformity across the surfaces. Finally, velocity profiles are explored to assess flow behavior, including turbulence and streamline patterns, which play a critical role in determining overall heat transfer efficiency. By systematically examining these four aspects for each pattern, this section aims to provide a detailed comparison of their respective strengths and limitations, offering valuable insights into how design characteristics influence thermal and hydrodynamic performance.

Pattern 1

Figure 3 presents a color-coded representation of the surface Nusselt number (Nu) at a specific location, indicated as 100 μm. The Nusselt number is a dimensionless quantity used in heat transfer to characterize convective heat transfer between a fluid and a solid surface. In this figure, the Nu values are visualized using a gradient color scale, where higher Nu values are represented by warmer colors (e.g., red) and lower or negative Nu values are depicted by cooler colors (e.g., blue). The central region of the plot shows a predominantly high Nu value, indicating strong convective heat transfer, while the edges exhibit a range of values, including some negative regions, suggesting variations in heat transfer efficiency across the surface. The presence of outliers (marked by small squares) indicates points with significantly different Nu values compared to the surrounding area, which could be due to localized effects such as boundary conditions or flow disturbances. Overall, the figure provides insight into the spatial distribution of heat transfer characteristics at the specified location.

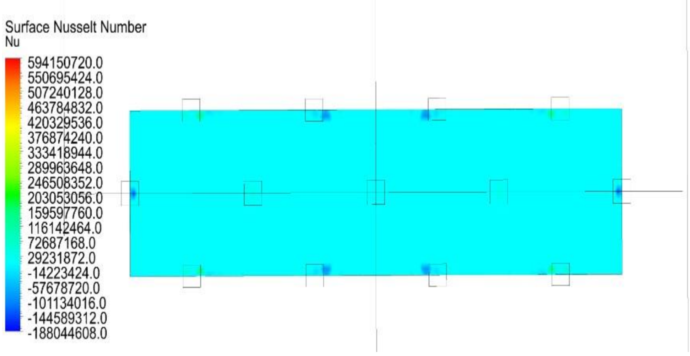

Figure 3: surface Nusselt Number at 100µm

The Figure 4 depicts the average surface Nusselt number distribution at 100 µm along the Z -axis for three distinct patterns, labeled as Pattern 1, Pattern 2, and Pattern 3. All three patterns exhibit oscillatory behavior, reflecting periodic fluctuations in heat transfer efficiency along the surface. Pattern 1 consistently shows the highest Nusselt number values, with pronounced peaks and troughs, indicating superior convective heat transfer compared to the other patterns. Pattern 2 demonstrates intermediate Nusselt numbers, with oscillations that are less extreme than those of Pattern 1 but more pronounced than Pattern 3. Pattern 3, on the other hand, displays the lowest Nusselt numbers, with smoother and less intense fluctuations, suggesting relatively lower heat transfer efficiency. Across all patterns, the Nusselt number varies significantly along the Z -axis, starting with high values at Z=0 and fluctuating periodically thereafter. These variations highlight the impact of the specific pattern geometry on heat transfer characteristics, with Pattern 1 offering the most efficient heat transfer and Pattern 3 the least. Overall, the oscillatory trends emphasize the non-uniform nature of heat transfer along the surface, influenced by the interplay of flow dynamics and surface design.

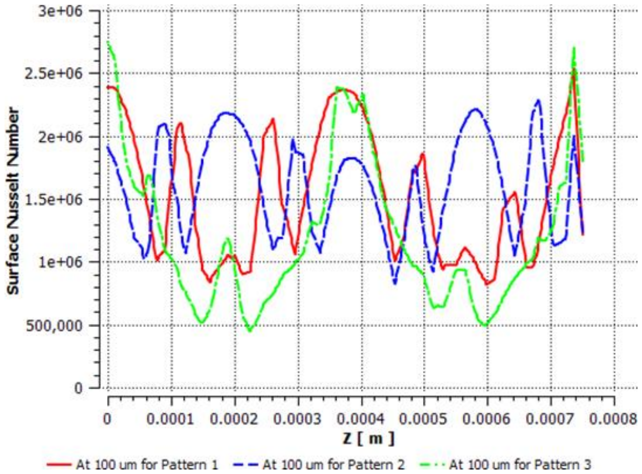

Figure 4: Average Surface Nusselt Number Distribution pattern at 100 µm

Figure 5 illustrates the 2-D pressure contour at a distance of 100 µm, providing a detailed visualization of the pressure distribution across the surface. The color gradient represents varying pressure levels, with warmer colors like red and yellow indicating regions of high pressure, while cooler colors such as green and blue signify lower pressure zones. The numerical scale reveals a wide range of pressure values, from approximately 29558.64 Pa at the highest to −1259.8 Pa at the lowest, emphasizing significant spatial variations in pressure. The contour exhibits a symmetrical and periodic pattern, with localized high-pressure regions appearing as bright yellow or red spots distributed evenly across the surface. These high-pressure zones are likely caused by flow compression or stagnation points where the fluid encounters resistance due to the geometry. Between these regions, areas of lower pressure, depicted by cooler colors, suggest flow expansion or increased velocity, consistent with Bernoulli's principle. The alternating pattern of high and low-pressure zones highlights the intricate interplay between the surface design and flow dynamics, with the geometry playing a key role in shaping the pressure field. Overall, the figure underscores the complex relationship between the pattern’s structure and the resulting pressure distribution, offering valuable insights into how localized pressure variations influence fluid behavior and heat transfer efficiency at this specific distance.

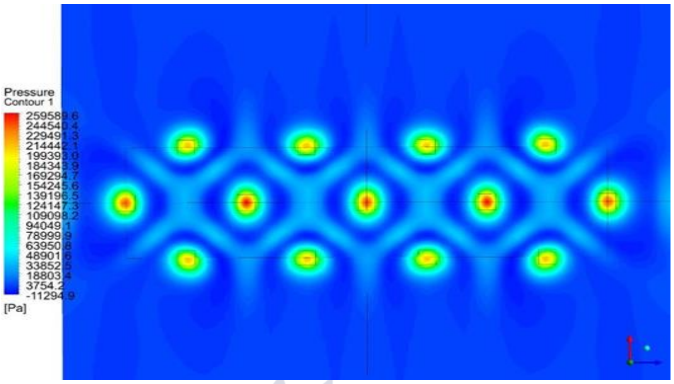

Figure 5: 2-D Pressure Contour at 100 μm Distance

Figure 6 provides a 3D pressure contour at a distance of 100 μm, offering a detailed three-dimensional visualization of the pressure distribution across the surface. The color gradient represents varying pressure levels, with warmer colors such as red and yellow indicating regions of high pressure, while cooler colors like blue signify areas of lower pressure. The numerical scale highlights significant variations in pressure, ranging from approximately 24521.16 Pa at the highest to −1259.8 Pa at the lowest, emphasizing the complexity of the pressure field. The 3D perspective reveals a symmetrical and periodic pattern of localized high-pressure zones, appearing as elevated peaks or ridges, interspersed with low-pressure valleys depicted by cooler colors. These high-pressure regions are likely caused by flow compression or stagnation points where the fluid encounters resistance due to the geometry, while the low-pressure zones suggest flow expansion or increased velocity. The consistent spacing and symmetry of these pressure variations reflect the influence of the pattern's design on the fluid dynamics, demonstrating how the geometry shapes the pressure contours. The vertical dimension in the 3D plot further accentuates the magnitude of pressure gradients, highlighting the pronounced differences between high-pressure peaks and low-pressure depressions. Overall, this figure underscores the intricate relationship between the surface design and the resulting pressure distribution, providing valuable insights into how localized pressure variations impact flow behavior and thermal performance.

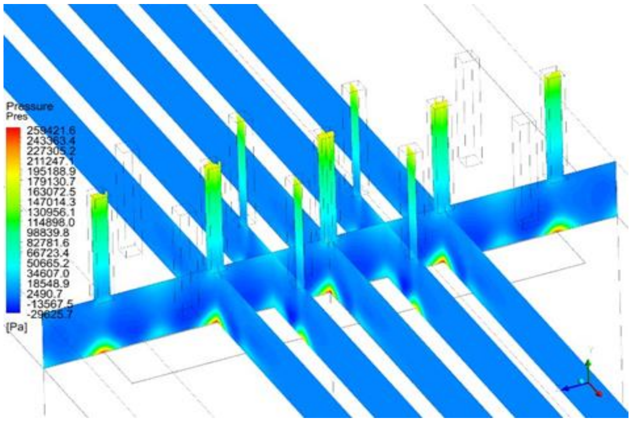

Figure 6: 3D Pressure Contour at 100 μm Distance

Figure 7 illustrates the pressure distribution at a distance of 100 μm along the Z -axis for three distinct patterns: Pattern 1, Pattern 2, and Pattern 3. Each pattern exhibits unique trends in pressure variation, reflecting differences in flow dynamics and fluid behavior. Pattern 1 (red line) demonstrates moderate fluctuations in pressure, with sharp peaks and troughs that suggest turbulent or highly dynamic flow conditions. Notably, near Z=0.007 m, there is a significant dip where the pressure drops sharply, indicating a localized region of reduced pressure. In contrast, Pattern 2 (blue line) shows the most stable behavior among the three, with relatively smooth and consistent pressure variations. The blue curve exhibits fewer extreme fluctuations, suggesting less turbulent flow conditions and a more uniform pressure field along the Z -axis. On the other hand, Pattern 3 (green line) displays the most dramatic pressure variations, characterized by pronounced oscillations and extreme peaks. Near Z=0.007 m, the green curve reaches an exceptionally high peak, indicating a localized region of intense pressure buildup, while also showing regions of negative pressure elsewhere. These significant fluctuations highlight the dynamic nature of Pattern 3's flow behavior. Overall, the graph underscores the influence of pattern geometry on pressure distribution, with Pattern 1 striking a balance between stability and variability, Pattern 2 maintaining consistent and stable pressure conditions, and Pattern 3 exhibiting highly erratic and intense pressure changes. This analysis highlights how design choices impact fluid dynamics, with each pattern showcasing distinct characteristics that influence flow stability and pressure efficiency. Figure 11 highlights the pressure behavior at a distance of 100 μm for three distinct patterns, providing insights into their respective turbulence levels. For Pattern 1, the pressure ranges between 10,000 Pa and 40,000 Pa, indicating moderate fluctuations and a balance between stability and variability in flow dynamics. This suggests that Pattern 1 experiences moderate turbulence, with neither excessively chaotic nor completely uniform flow conditions. In contrast, Pattern 2 demonstrates the least turbulence, as its pressure varies between -10,000 Pa and 40,000 Pa, including regions of negative pressure values that reflect relatively stable and less turbulent flow. The smoother pressure trend underscores its ability to maintain consistent flow conditions. On the other hand, Pattern 3 exhibits the highest turbulence, with pressure values spanning from 10,000 Pa to 60,000 Pa, including a dramatic spike near Z=0.007 m. These extreme fluctuations and localized high-pressure regions highlight highly dynamic and chaotic flow behavior. Overall, the analysis reveals a clear progression in turbulence levels: Pattern 3 experiences the most intense turbulence, followed by Pattern 1 with moderate turbulence, while Pattern 2 remains the most stable with the least turbulence. This comparison emphasizes how the design of each pattern significantly influences fluid dynamics and pressure distribution.

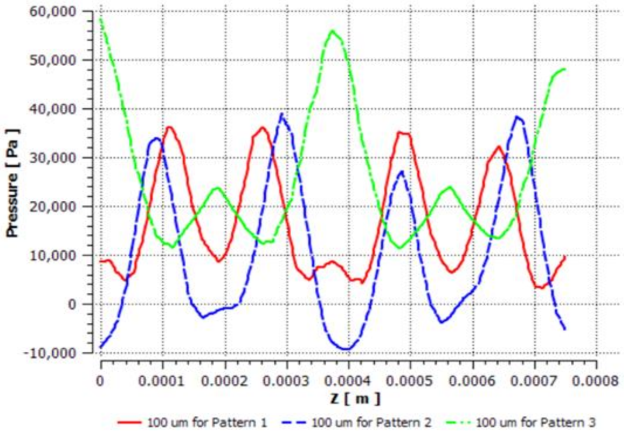

Figure 7: Pressure Distribution at 100 µm Distance

Figure 8 illustrates the temperature distribution at a distance of 100 µm for Pattern 1 , using a color gradient to visualize how temperature varies across the surface. The warmer colors, such as red and yellow, represent regions of higher temperatures, while cooler colors like blue and green indicate areas of lower temperatures. The numerical scale highlights significant temperature variations, ranging from approximately 41.6 °C at the highest to 11.7 °C at the lowest. The contour reveals a symmetrical and periodic pattern, with localized high-temperature zones appearing as bright yellow or red spots distributed evenly across the surface. These high-temperature regions are likely caused by heat accumulation or stagnation points where thermal energy is concentrated due to the geometry or flow conditions. Between these hotspots, cooler regions depicted by green and blue suggest effective heat dissipation or reduced thermal energy in those areas. The alternating pattern of high and low temperatures emphasizes the complex interaction between the surface design and thermal behavior, highlighting how geometry influences heat transfer dynamics. Compared to other patterns (based on previous observations), Pattern 1 demonstrates a balance between stability and variability, with an organized structure of localized hotspots and cooler zones. This contrasts with potentially more uniform temperature distributions in Pattern 2 or highly erratic fluctuations in Pattern 3. Overall, this figure underscores how the design of Pattern 1 creates a structured yet dynamic thermal profile, reflecting its role in shaping both localized heat accumulation and overall thermal efficiency.

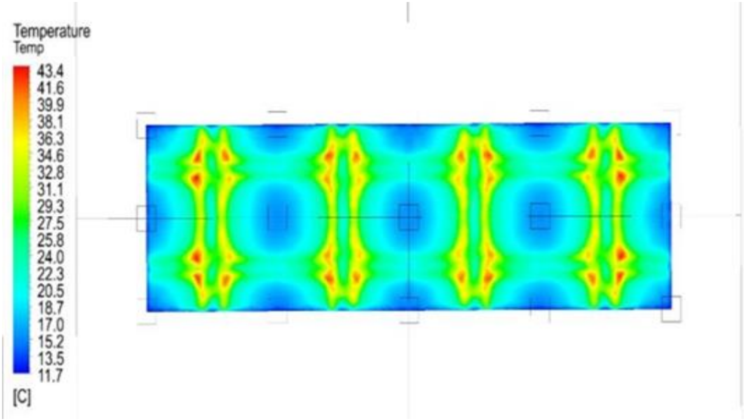

Figure 8:Showing Temperature Distribution at 100 µm

Figure 9 illustrates the temperature distribution at a distance of 100 μm along the Z -axis for three distinct patterns: Pattern 1, Pattern 2, and Pattern 3, providing insights into their respective thermal behaviors. The graph reveals oscillatory trends in all three patterns, with temperatures ranging from approximately 15 °C to over 35 °C, highlighting significant spatial variations. Pattern 1 (red line) exhibits moderate fluctuations, with sharp peaks and troughs that suggest dynamic heat transfer conditions. Notably, near Z=0.007 m, there is a sharp drop in temperature, indicating localized cooling or reduced heat accumulation. In contrast, Pattern 2 (blue line) demonstrates the most stable behavior, with relatively smooth and consistent temperature variations. While some fluctuations are present, they are less pronounced than in Pattern 1, reflecting more uniform heat transfer conditions. On the other hand, Pattern 3 (green line) displays the most erratic behavior, characterized by dramatic oscillations and extreme peaks. Near Z=0.007 m, the green curve reaches an exceptionally high temperature, suggesting intense localized heat buildup, while also showing regions of lower temperature elsewhere. These significant fluctuations underscore the highly dynamic thermal behavior of Pattern 3. Overall, the graph highlights how the geometry of each pattern influences temperature distribution: Pattern 1 strikes a balance between stability and variability, Pattern 2 maintains consistent and stable thermal conditions, and Pattern 3 exhibits pronounced instability with localized hotspots. This analysis emphasizes the critical role of design in shaping thermal dynamics, with each pattern showcasing unique characteristics that impact heat transfer efficiency and thermal uniformity.

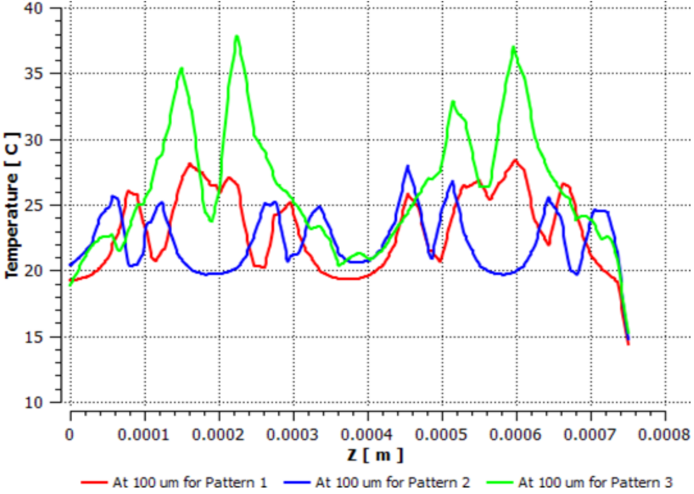

Figure 9: Temperature Distribution at 100 μm Distance

Figure 10 illustrates the inlet jet velocity at a distance of 100 μm for Pattern 1 , using a color gradient to visualize how velocity varies across the surface. The warmer colors, such as red and yellow, represent regions of higher velocity, while cooler colors like blue and green indicate areas of lower velocity. The numerical scale highlights significant velocity variations, ranging from approximately 24.7 m/s at the highest to much lower values in certain regions. The contour reveals a symmetrical and periodic pattern, with localized high-velocity zones appearing as bright yellow or red spots distributed evenly across the surface. These high-velocity regions are likely caused by flow acceleration or geometric features that channel fluid into specific areas. Between these zones, cooler regions depicted by green and blue suggest flow deceleration or reduced fluid speed, possibly due to flow expansion or resistance.

The figure shows that the inlet jet velocity is decreased at 100 μm distance. It was observed that as the distance from the centerline increases, the inlet jet velocity decreases, and vice versa. This trend indicates that the flow experiences greater deceleration or diffusion away from the centerline, where velocities are typically higher due to more concentrated flow paths. The alternating pattern of high and low velocities emphasizes the complex interaction between the surface design and fluid dynamics, highlighting how geometry influences flow behavior. Compared to other patterns (based on previous observations), Pattern 1 demonstrates a balance between stability and variability, with an organized structure of localized high-speed regions interspersed with areas of slower flow. This contrasts with potentially more uniform velocity distributions in Pattern 2 or highly erratic fluctuations in Pattern 3. Overall, this figure underscores how the design of Pattern 1 creates a structured yet dynamic velocity profile, reflecting its role in shaping both localized flow acceleration and overall fluid behavior.

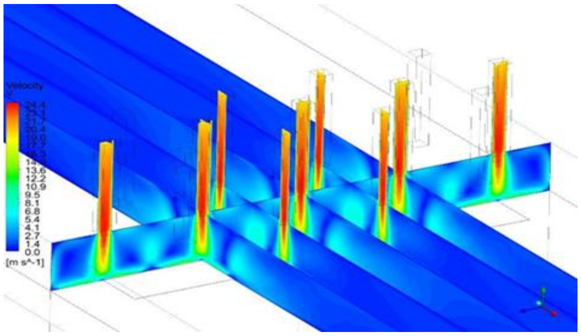

Figure 10: Inlet Jet Velocity at 100 μm Distance

Pattern 2

Figure 11 illustrates the surface Nusselt number (Nu) distribution at the centerline for Pattern 2, with a color gradient representing varying Nu values. Warmer colors, such as red, correspond to higher Nu values, while cooler colors, like blue, indicate lower or even negative Nu values. The central region of the plot predominantly shows high Nu values, suggesting strong convective heat transfer at this location. However, compared to the data observed at a distance of 100 μm, the turbulence factor at the centerline is notably reduced. This is evidenced by the relatively smoother and more uniform distribution of Nu values, with fewer extreme fluctuations or localized variations. While some outliers (marked by small squares) are still present, indicating areas with significant deviations in heat transfer efficiency, the overall trend suggests a more stable flow environment at the centerline. The reduced turbulence leads to less chaotic heat transfer characteristics, contrasting with the likely higher turbulence and greater variability observed at the 100-μm distance. Thus, Figure 5 highlights how flow stability directly impacts heat transfer behavior, with the centerline exhibiting a more controlled and consistent pattern of heat exchange.

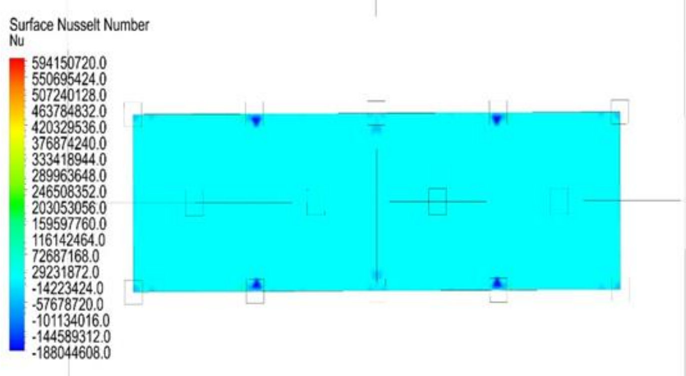

Figure 11: Nusselt Number at Centerline

The Figure 12 illustrates the surface Nusselt number (Nu) distribution along the Z -axis at the centerline for three distinct patterns: Pattern 1, Pattern 2, and Pattern 3. Pattern 1 (red line) exhibits highly dynamic behavior, characterized by sharp fluctuations with significant peaks and troughs. Notably, near Z=0.007 m, the Nusselt number for Pattern 1 drops dramatically to negative values, indicating regions of reversed or highly inefficient heat transfer. This suggests that Pattern 1 experiences turbulent and unstable flow conditions, leading to extreme variability in convective heat transfer efficiency. In contrast, Pattern 2 (blue line) demonstrates moderate fluctuations, showing a more stable trend compared to Pattern 1. While some peaks and troughs are present, the overall behavior is less erratic, implying a balance between turbulence and stability. Pattern 3 (green line), on the other hand, remains nearly constant and close to zero throughout the Z -axis, indicating minimal convective heat transfer activity. This suggests that Pattern 3's geometry or flow conditions do not promote effective heat exchange, resulting in consistently low Nusselt numbers. Collectively, these trends highlight how the design of each pattern significantly influences heat transfer efficiency and turbulence levels, with Pattern 1 being the most turbulent, Pattern 2 offering moderate stability, and Pattern 3 demonstrating negligible heat transfer activity.

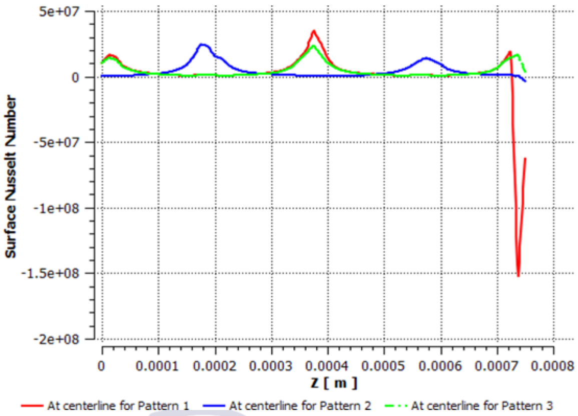

Figure 12: Average Surface Nusselt Number Distribution Pattern at Centerline

Figure 13 presents a 2-D pressure contour at the centerline for Pattern 2 , offering a detailed visualization of the pressure distribution across the surface. The color gradient represents varying pressure levels, with warmer colors such as red and yellow indicating high-pressure regions, while cooler colors like green and blue signify areas of lower pressure. The numerical scale reveals a pressure range from approximately 53454.22 Pa at the highest to −1259.8 Pa at the lowest, emphasizing significant spatial variations in pressure. The contour exhibits a symmetrical and periodic pattern, with localized high-pressure zones appearing as bright yellow or red spots distributed evenly across the surface. These high-pressure regions are likely caused by flow compression or stagnation points where the fluid encounters resistance due to the geometry. Between these zones, areas of lower pressure, depicted by cooler colors, suggest flow expansion or increased velocity, consistent with Bernoulli's principle. The alternating pattern of high and low-pressure regions highlights the intricate interplay between the surface design and flow dynamics, with the geometry playing a key role in shaping the pressure field. Compared to other patterns, Pattern 2 demonstrates a more stable and controlled pressure distribution, reflecting less turbulence and more uniform flow conditions than the highly dynamic behavior observed in Pattern 1 or the erratic fluctuations seen in Pattern 3. Overall, this figure underscores how the design of Pattern 2 influences its fluid dynamics, resulting in a smoother and more consistent pressure profile that enhances flow stability and reduces turbulence.

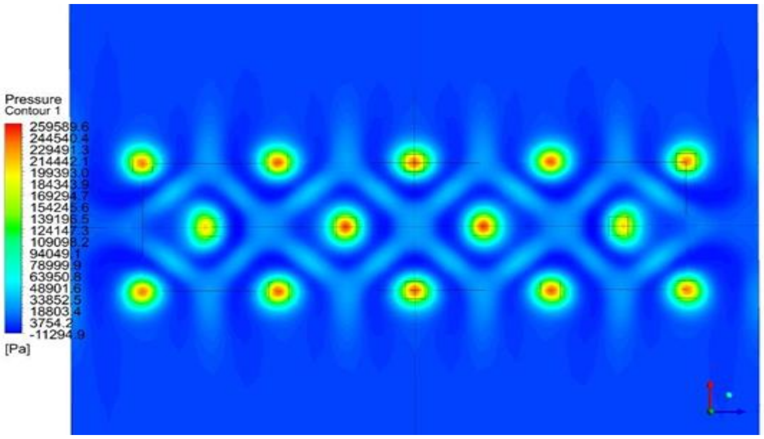

Figure 13: 2-D Pressure Contour at Centerline

Figure 14 provides a 3-D view of the pressure distribution at the centerline, offering a detailed and immersive visualization of how pressure varies across the surface. The color gradient represents pressure levels, with warmer colors like red and yellow indicating high-pressure regions, while cooler colors such as green and blue signify areas of lower pressure. The numerical scale highlights significant variations in pressure, ranging from approximately 25421.6 Pa at the highest to −1259.8 Pa at the lowest. The 3D perspective reveals a symmetrical and periodic pattern of localized high-pressure zones, appearing as elevated peaks or ridges interspersed with low-pressure valleys depicted by cooler colors. These high-pressure regions are likely caused by flow compression or stagnation points where fluid encounters resistance due to the geometry, while the low-pressure areas suggest flow expansion or increased velocity, consistent with Bernoulli's principle. Compared to the 2D contour (Figure 12), this 3D representation adds depth to the analysis, emphasizing the vertical extent of pressure variations and providing a clearer understanding of the spatial distribution of pressure gradients. The alternating pattern of high and low-pressure regions reflects the interplay between the surface design and flow dynamics, underscoring the role of geometry in shaping the pressure field. Overall, this figure reinforces the stability and controlled nature of Pattern 2, with fewer extreme fluctuations and a more uniform pressure profile compared to other patterns, indicative of reduced turbulence and consistent flow behavior. This detailed visualization highlights how the design influences fluid dynamics and contributes to efficient and predictable pressure distribution.

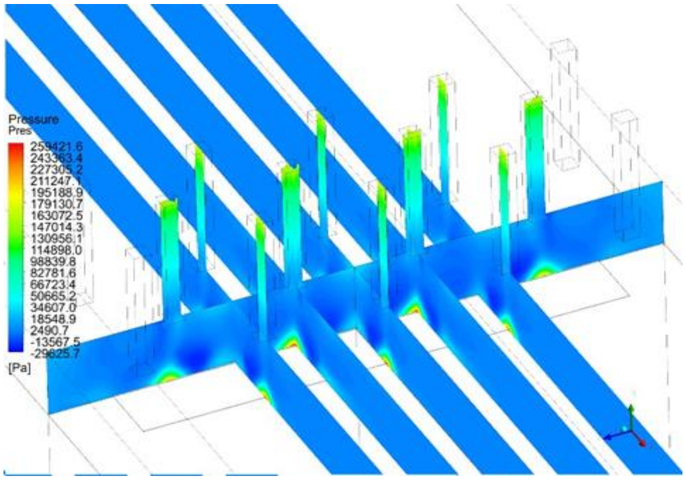

Figure 14: 3-D view of Pressure at Centerline

Figure 15 illustrates the pressure distribution at the centerline along the Z -axis for three distinct patterns: Pattern 1, Pattern 2, and Pattern 3. Each pattern exhibits unique trends in pressure variation, reflecting differences in flow dynamics and fluid behavior. Pattern 1 (red line) demonstrates moderate fluctuations in pressure, with sharp peaks and troughs that suggest turbulent or highly dynamic flow conditions. Notably, near Z=0.007 m, there is a significant dip where the pressure drops sharply, indicating a localized region of reduced pressure. In contrast, Pattern 2 (blue line) shows the most stable behavior among the three, with relatively smooth and consistent pressure variations. The blue curve exhibits fewer extreme fluctuations, suggesting less turbulent flow conditions and a more uniform pressure field along the Z -axis. On the other hand, Pattern 3 (green line) displays the most dramatic pressure variations, characterized by pronounced oscillations and extreme peaks. Near Z=0.007 m, the green curve reaches an exceptionally high peak, indicating a localized region of intense pressure buildup, while also showing regions of negative pressure elsewhere. These significant fluctuations highlight the dynamic nature of Pattern 3's flow behavior. Overall, the graph underscores the influence of pattern geometry on pressure distribution, with Pattern 1 striking a balance between stability and variability, Pattern 2 maintaining consistent and stable pressure conditions, and Pattern 3 exhibiting highly erratic and intense pressure changes. This analysis highlights how design choices impact fluid dynamics, with each pattern showcasing distinct characteristics that influence flow stability and pressure efficiency.

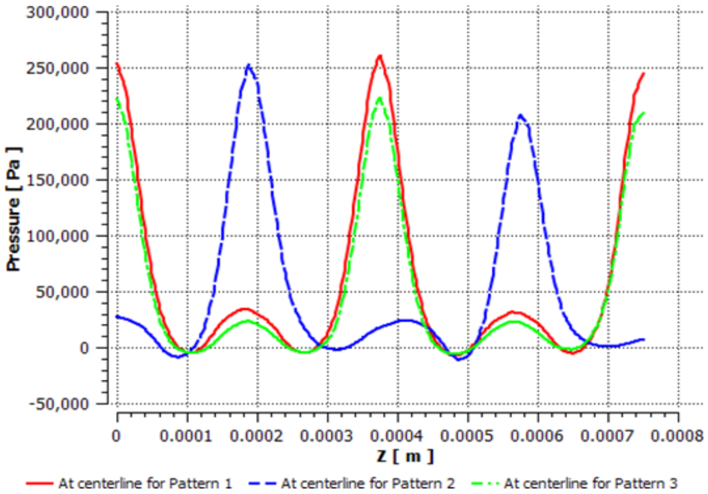

Figure 15: Pressure Distribution at Centerline

Figure 16 illustrates the temperature distribution at the centerline for Pattern 2 , using a color gradient to visualize how temperature varies across the surface. The warmer colors, such as red and yellow, represent regions of higher temperatures, while cooler colors like blue and green indicate areas of lower temperatures. The numerical scale highlights significant temperature variations, ranging from approximately 43.4 °C at the highest to 11.7 °C at the lowest. The contour reveals a symmetrical and periodic pattern, with localized high-temperature zones appearing as bright yellow or red spots distributed evenly across the surface. These high-temperature regions are likely caused by heat accumulation or stagnation points where thermal energy is concentrated due to the geometry or flow conditions. Between these hotspots, cooler regions depicted by green and blue suggest effective heat dissipation or reduced thermal energy in those areas. The alternating pattern of high and low temperatures emphasizes the complex interaction between the surface design and thermal behavior, highlighting how geometry influences heat transfer dynamics. Compared to other patterns (based on previous observations), Pattern 2 demonstrates a relatively stable and uniform temperature profile, with fewer extreme fluctuations compared to the more dynamic behavior of Pattern 1 or the erratic oscillations of Pattern 3. This structured thermal distribution reflects Pattern 2’s ability to maintain consistent heat transfer conditions, balancing localized heat buildup with effective dissipation. Overall, this figure underscores how the design of Pattern 2 creates a predictable and efficient thermal profile, emphasizing its role in shaping both localized and overall thermal performance.

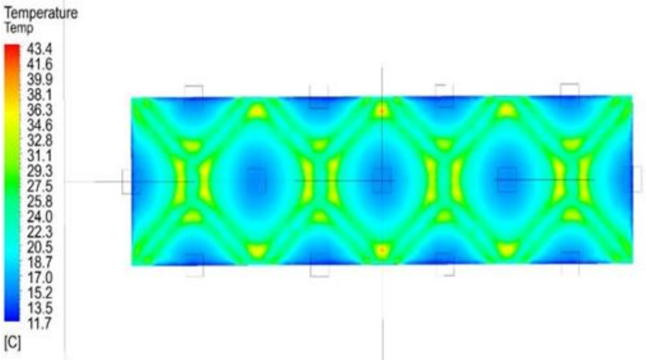

Figure 16: Showing Temperature Distribution at Centerline

From the below Figure 17, it can be seen that for Pattern 1 and Pattern 3 , the temperature increases from approximately 15°C to 35°C along the Z -axis. However, as the distance increases beyond Z=0.0007 m, there is a sudden drop in temperature, indicating localized cooling or reduced heat accumulation in these regions. This behavior suggests that both Pattern 1 and Pattern 3 experience significant fluctuations in temperature, with intense heat buildup followed by sharp reductions, likely due to specific geometric features or flow dynamics. In contrast, Pattern 2 exhibits a different trend, where the overall temperature decreases steadily from around 45°C to 20°C as the distance along the Z -axis increases. This smooth and consistent decrease in temperature reflects a more uniform heat transfer process, where heat dissipation occurs gradually without the pronounced spikes or drops observed in Patterns 1 and 3. The relatively stable thermal profile of Pattern 2 highlights its design's effectiveness in maintaining consistent temperature conditions across the surface, emphasizing its ability to promote steady and predictable thermal behavior compared to the more dynamic and erratic trends of the other patterns.

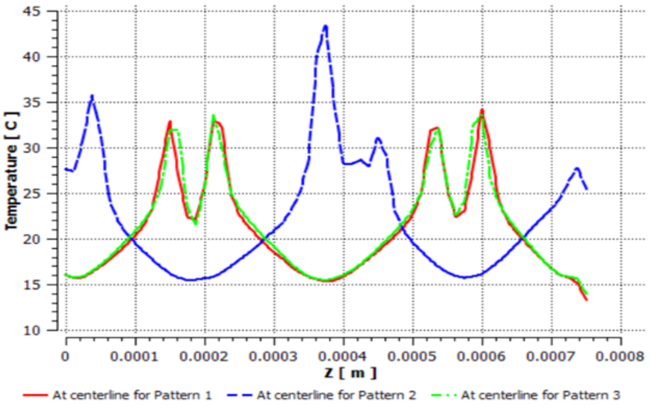

Figure 17: Temperature Distribution at Centerline

Figure 18 illustrates the inlet jet velocity at the centerline for Pattern 2 , using a color gradient to visualize how velocity varies across the surface. The warmer colors, such as red and yellow, represent regions of higher velocity, while cooler colors like blue and green indicate areas of lower velocity. The numerical scale highlights significant velocity variations, ranging from approximately 24.7 m/s at the highest to much lower values in certain regions. The contour reveals a symmetrical and periodic pattern, with localized high-velocity zones appearing as bright yellow or red spots distributed evenly across the surface. These high-velocity regions are likely caused by flow acceleration or geometric features that channel fluid into specific areas, while the cooler regions depicted by green and blue suggest flow deceleration or reduced fluid speed, possibly due to flow expansion or resistance. Compared to other patterns (based on previous observations), Pattern 2 demonstrates a relatively stable and uniform velocity profile, with fewer extreme fluctuations compared to the more dynamic behavior of Pattern 1 or the erratic oscillations of Pattern 3. This structured velocity distribution reflects Pattern 2’s ability to maintain consistent flow conditions, balancing localized high-speed regions with areas of slower flow. Overall, this figure underscores how the design of Pattern 2 creates a predictable and efficient flow profile, emphasizing its role in shaping both localized and overall fluid dynamics.

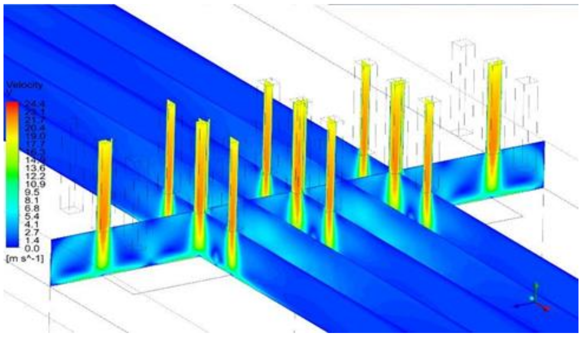

Figure 18: Inlet Jet Velocity at centerline

Pattern 3

Figure 19 illustrates the surface Nusselt number (Nu) distribution at the edges for Pattern 3 , using a color gradient to represent Nu values. The plot is dominated by light blue hues, indicating consistently low or near-zero Nusselt numbers across most of the surface, which reflects minimal convective heat transfer activity at the edges. While there are a few localized outliers marked by small squares, these deviations remain minor and do not significantly alter the overall trend of negligible heat transfer efficiency. The numerical labels on the left side of the plot further confirm this observation, showing extremely low Nu values, such as −1.8×106 to −1.4×106 , which align with the trends observed at the centerline in previous figures. This uniformity suggests that the geometry or flow conditions associated with Pattern 3 result in consistently poor heat transfer performance, both at the edges and across the entire surface. In comparison to other patterns, which may exhibit dynamic fluctuations or moderate heat transfer activity, Pattern 3 stands out as the least efficient, with its edges showing no significant improvement in convective heat transfer. Overall, the figure reinforces the conclusion that Pattern 3's design inherently limits its ability to promote effective heat exchange, making it the least effective among the patterns analyzed.

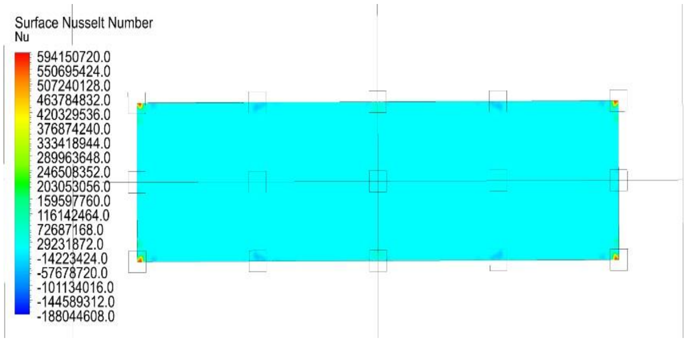

Figure 19: Surface Nusselt Number at Edges

Figure 20 illustrates the average surface Nusselt number (Nu) distribution along the Z -axis at the edges for three distinct patterns: Pattern 1, Pattern 2, and Pattern 3. Each pattern exhibits unique heat transfer characteristics as Z increases. Pattern 1 (red line) shows moderate fluctuations in Nu values, with some peaks and troughs that indicate variability in convective heat transfer efficiency. Notably, near Z=0.007 m, there is a sharp drop in Nu values, suggesting localized regions of reduced or reversed heat transfer. In contrast, Pattern 2 (blue line) demonstrates exceptional stability, with minimal fluctuations and a nearly flat trend throughout the Z -axis, reflecting consistent heat transfer efficiency along the edges. This indicates that Pattern 2's design promotes uniform flow conditions, resulting in steady heat transfer performance. On the other hand, Pattern 3 (green line) displays highly dynamic behavior, characterized by significant oscillations and extreme peaks. Most notably, near Z=0.007 m, Pattern 3 experiences a dramatic spike in Nu values, reaching very high positive values, which suggests a localized region of intense heat transfer activity. Outside this peak, however, Pattern 3's Nu values remain low and inconsistent, with both positive and negative regions indicating sporadic heat transfer efficiency. Overall, the graph highlights the contrasting effects of pattern geometry on heat transfer: Pattern 1 strikes a balance between stability and variability, Pattern 2 excels in maintaining uniform heat transfer, and Pattern 3 shows sporadic but intense heat transfer in localized areas, particularly near Z=0.007 m. These differences underscore how design influences turbulence and convective heat transfer efficiency at the edges.

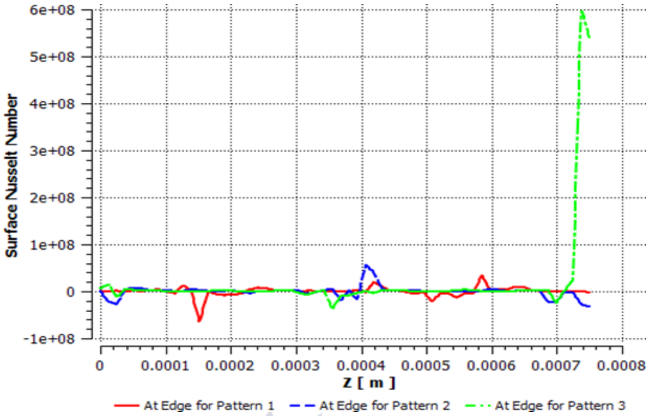

Figure 20: Average Surface Nusselt Number Distribution Pattern at Edges

Figure 21 presents the 2-D pressure contour at the edges for Pattern 3 , offering a detailed visualization of the pressure distribution across the surface. The color gradient represents varying pressure levels, with warmer colors such as red and yellow indicating high-pressure regions, while cooler colors like blue and green signify areas of lower pressure. The numerical scale highlights significant pressure variations, ranging from approximately 29558.64 Pa at the highest to −1259.8 Pa at the lowest. The contour reveals a symmetrical yet highly dynamic pattern, with localized high-pressure zones appearing as bright yellow or red spots distributed across the surface. These high-pressure regions are likely caused by flow compression or stagnation points where fluid encounters resistance due to the geometry. Between these zones, low-pressure areas depicted by cooler colors suggest flow expansion or increased velocity, consistent with Bernoulli's principle. The alternating pattern of high and low-pressure regions emphasizes the complex interaction between the surface design and flow dynamics, highlighting how geometry influences the pressure field. Compared to other patterns, Pattern 3 exhibits significantly more pronounced fluctuations, with sharp peaks and deep troughs that indicate intense turbulence and uneven flow behavior. This contrasts with the relatively stable pressure profiles observed in Patterns 1 and 2, underscoring the erratic nature of Pattern 3's design. Overall, this figure underscores the highly turbulent flow conditions at the edges of Pattern 3, characterized by localized pressure spikes and significant spatial variability, reflecting the influence of its geometry on creating complex and unstable flow patterns.

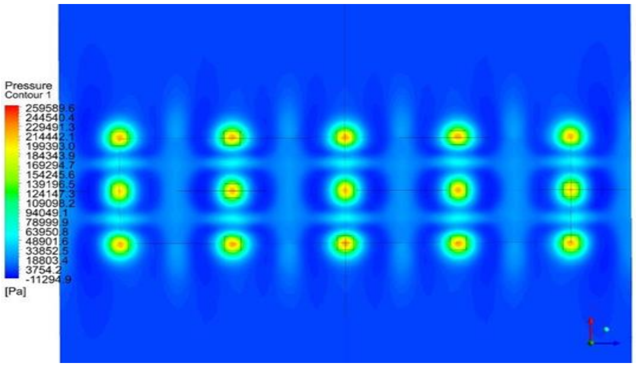

Figure 21:2-D Pressure Contour at Edges

Figure 22 provides a 3-D view of the pressure distribution at the edges for Pattern 3 , offering a detailed and immersive visualization of how pressure varies spatially across the surface. The color gradient represents pressure levels, with warmer colors like red and yellow indicating high-pressure regions, while cooler colors such as blue and green signify low-pressure areas. This three-dimensional perspective highlights both horizontal and vertical trends in the pressure field, emphasizing significant spatial variations. The 3D contour reveals localized high-pressure zones appearing as elevated peaks or ridges, interspersed with deep low-pressure valleys depicted by cooler colors. These high-pressure regions likely result from flow compression or stagnation points caused by the geometry, while the low-pressure areas suggest flow expansion or increased velocity, consistent with Bernoulli's principle. Compared to earlier patterns, Pattern 3 demonstrates far more pronounced fluctuations, with sharp peaks and deep troughs that indicate intense turbulence and uneven flow behavior. In contrast, Pattern 1 exhibited moderate fluctuations, showing a balance between stability and variability, while Pattern 2 displayed a stable and nearly flat pressure profile, reflecting minimal turbulence. The extreme oscillations in Pattern 3 highlight its highly dynamic and erratic nature, underscoring how its design promotes complex and unstable flow conditions. This 3D visualization effectively captures the intricate relationship between geometry and fluid dynamics, showcasing how Pattern 3's edges experience localized pressure spikes and significant variability, unlike the smoother and more predictable pressure distributions observed in Patterns 1 and 2.

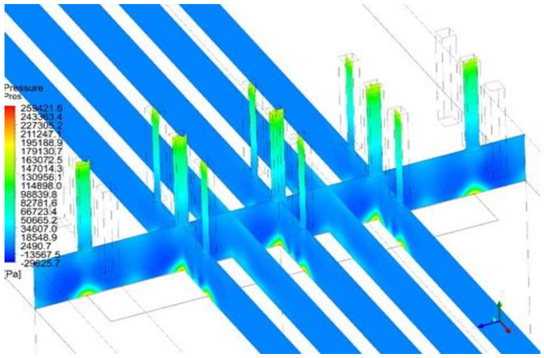

Figure 22: 3-D View of Pressure at Edges

Figure 23 illustrates the pressure distribution at the edges along the Z -axis for three distinct patterns: Pattern 1, Pattern 2, and Pattern 3, providing insights into their respective flow dynamics. The graph reveals oscillatory behavior in all three patterns, with pressure values spanning a wide range, from approximately −50,000 Pa to over 250,000 Pa, highlighting significant spatial variations. Pattern 1 (red line) exhibits moderate fluctuations, with sharp peaks and troughs that suggest turbulent or dynamic flow conditions. Notably, near Z=0.007 m, there is a sharp drop in pressure, indicating localized regions of reduced pressure. In contrast, Pattern 2 (blue line) demonstrates the most stable behavior, with relatively smooth and consistent pressure variations. While some fluctuations are present, they are less pronounced than in Pattern 1, reflecting less turbulent flow conditions. On the other hand, Pattern 3 (green line) displays the most erratic behavior, characterized by dramatic oscillations and extreme peaks. Near Z=0.007 m, the green curve reaches an exceptionally high peak, suggesting intense localized pressure buildup, while also showing regions of negative pressure elsewhere. These significant fluctuations underscore the highly dynamic nature of Pattern 3's flow behavior. Overall, the graph highlights how the geometry of each pattern influences pressure distribution: Pattern 1 strikes a balance between stability and variability, Pattern 2 maintains consistent and stable pressure conditions, and Pattern 3 exhibits pronounced turbulence and pressure spikes. This analysis emphasizes the critical role of design in shaping fluid dynamics and pressure profiles, with each pattern showcasing unique characteristics that impact flow stability and efficiency.

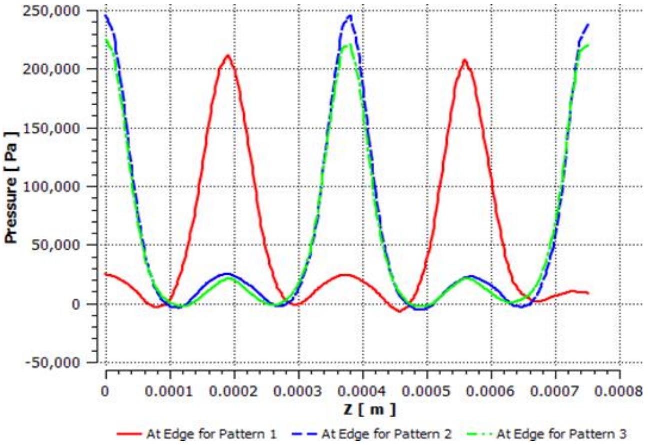

Figure 23: Pressure Distribution at Edges

Figure 24 illustrates the temperature distribution at the edges for Pattern 3 , using a color gradient to visualize how temperature varies across the surface. The warmer colors, such as red and yellow, represent regions of higher temperatures, while cooler colors like blue and green indicate areas of lower temperatures. The numerical scale highlights significant temperature variations, ranging from approximately 43.4 °C at the highest to 11.7 °C at the lowest. The contour reveals a highly dynamic pattern, with localized high-temperature zones appearing as bright yellow or red spots distributed across the surface. These hotspots are likely caused by heat accumulation or stagnation points where thermal energy is concentrated due to the geometry or flow conditions. Between these high-temperature regions, cooler areas depicted by green and blue suggest effective heat dissipation or reduced thermal energy. The alternating pattern of high and low temperatures emphasizes the complex interaction between the surface design and thermal behavior, highlighting how geometry influences heat transfer dynamics. Compared to other patterns (based on previous observations), Pattern 3 demonstrates significantly more pronounced fluctuations, with sharp peaks and deep troughs that indicate intense and uneven thermal behavior. This contrasts with the relatively stable temperature profiles observed in Patterns 1 and 2, underscoring the erratic nature of Pattern 3's design. Overall, this figure underscores how the geometry of Pattern 3 creates a highly uneven thermal profile, characterized by localized heat buildup and sharp temperature gradients, reflecting its role in shaping complex and unstable thermal dynamics.

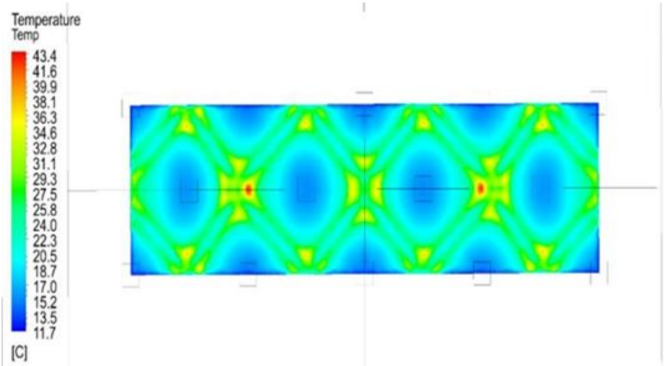

Figure 24: Temperature Distribution at Edges

In the below temperature contour Figure 25, the primitive value set at the inlet boundary condition of the coolant medium is a constant temperature of 10 °C . As the fluid flows along the surface, the temperature increases from 10 °C to 15 °C , indicating heat transfer occurring due to interactions between the fluid and the surface. Simultaneously, the volume flow rate of the fluid increases from 0.000247 m^3/s to 0.00247 m^3/s , reflecting changes in fluid dynamics as it moves through the system. This increase in flow rate suggests enhanced fluid movement, which can influence both heat transfer efficiency and pressure distribution.

As the temperature, pressure, and volume flow rate all increase from the initial position to the final position, there is a corresponding increase in the Reynolds number . The Reynolds number (Re) is a dimensionless quantity that characterizes the balance between inertial forces and viscous forces in fluid flow. An increase in the Reynolds number indicates a shift toward more turbulent flow conditions, which can enhance heat transfer but may also introduce greater pressure fluctuations and localized hotspots.

The observed trends in temperature, pressure, and flow rate collectively highlight the interplay between thermal and fluid dynamics in the system. The increasing temperature and flow rate suggest active heat transfer processes, while the rising Reynolds number underscores the transition toward more complex flow behavior, potentially leading to intensified turbulence and localized regions of high heat accumulation or pressure buildup. These observations emphasize the importance of understanding how boundary conditions, fluid properties, and geometry interact to shape the overall thermal and hydrodynamic performance of the system

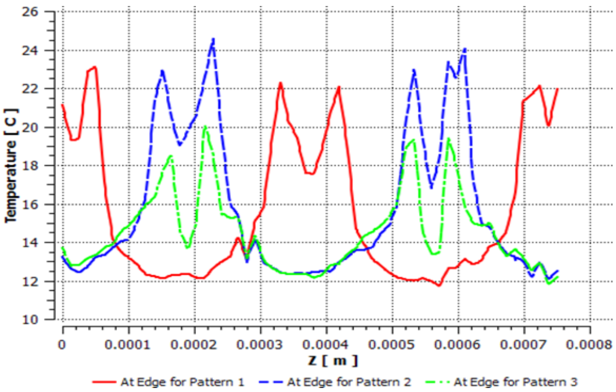

Figure 25: Temperature Distribution at Edge

Figure 26 illustrates the inlet jet velocity at the edges for Pattern 3 , using a color gradient to visualize how velocity varies across the surface. The warmer colors, such as red and yellow, represent regions of higher velocity, while cooler colors like blue and green indicate areas of lower velocity. The numerical scale highlights significant velocity variations, ranging from approximately 24.7 m/s at the highest to much lower values in certain regions. The contour reveals a highly dynamic pattern, with localized high-velocity zones appearing as bright yellow or red spots distributed across the surface. These high-velocity regions are likely caused by flow acceleration or geometric features that channel fluid into specific areas, while the cooler regions depicted by green and blue suggest flow deceleration or reduced fluid speed. Compared to other patterns (based on previous observations), Pattern 3 demonstrates significantly more pronounced fluctuations, with sharp peaks and deep troughs that indicate intense and uneven flow behavior. This contrasts with the relatively stable velocity profiles observed in Patterns 1 and 2, underscoring the erratic nature of Pattern 3's design. Overall, this figure underscores how the geometry of Pattern 3 creates a highly uneven velocity profile, characterized by localized high-speed regions and sharp velocity gradients, reflecting its role in shaping complex and unstable flow dynamics.

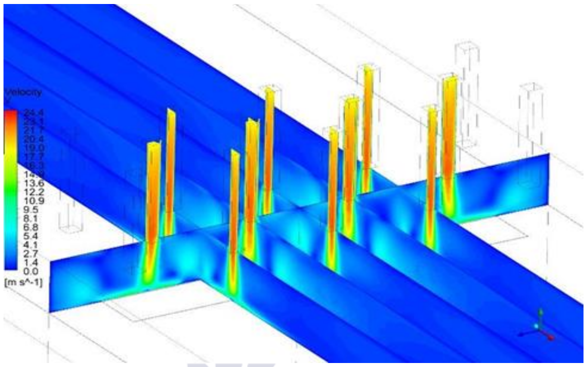

Figure 26: Inlet Jet Velocity at Edge

Summary of Thermal and Fluid Dynamics Performance Across Patterns

The performance of the three patterns Pattern 1, Pattern 2, and Pattern 3 can be comprehensively evaluated by analyzing key parameters such as pressure on the inlet jet, temperature distribution on the heater wall, and the surface Nusselt number. Table 3, the average pressure on the inlet jet reveals distinct trends across the three patterns. Pattern 1 exhibits the highest pressure at 213,371 Pa, indicating significant resistance or flow compression at the inlet. This high-pressure condition suggests that Pattern 1's geometry may create localized regions of flow stagnation or compression, leading to increased turbulence and dynamic flow behavior. Pattern 2, with an average pressure of 192,302 Pa, shows moderate pressure levels, reflecting a balance between flow stability and resistance. In contrast, Pattern 3 has the lowest pressure at 186,990 Pa, suggesting smoother fluid entry and reduced resistance. This lower pressure is likely due to its design promoting less restrictive flow pathways, which enhances fluid movement but may also These metrics provide a detailed understanding of how each pattern influences fluid dynamics, heat transfer efficiency, and thermal behavior.

Pressure on the Inlet Jet

From

contribute to uneven pressure distributions observed in earlier analyses.

Temperature Distribution on the Heater Wall

The area-averaged temperature on the heater wall, as shown in Table 4, highlights the thermal performance of each pattern. Pattern 3 exhibits the highest temperature at 26.82 °C, indicating significant heat accumulation or reduced heat dissipation efficiency. This elevated temperature suggests that while Pattern 3 achieves high heat transfer rates (as seen in the Nusselt number), it struggles to maintain thermal uniformity, potentially leading to localized overheating. On the other hand, Pattern 1 and Pattern 2 demonstrate more stable thermal profiles, with temperatures of 22.048 °C and

22.226 °C, respectively. These lower temperatures reflect better heat dissipation and more uniform thermal behavior, particularly for Pattern 2, which maintains consistent conditions across the surface. The higher temperature in Pattern 3 underscores a trade-off: while it excels in convective heat transfer, it may compromise thermal stability and uniformity.

Surface Nusselt Number on the Heater Wall

The area-averaged surface Nusselt number, presented in

Table 5, serves as a critical indicator of convective heat transfer efficiency. Pattern 3 achieves the highest Nusselt number at 4.29601×106, demonstrating superior convective heat transfer performance. This high value reflects the pattern's ability to enhance heat exchange, likely due to its geometry promoting turbulence and increased fluid interaction with the heater wall. Pattern 1, with a Nusselt number of 2.42394×106, shows moderate heat transfer efficiency, balancing thermal performance with relatively higher-pressure stability. In contrast, Pattern 2 exhibits the lowest Nusselt number at 1.87839×106, indicating less efficient heat transfer. However, this lower efficiency is offset by its stable thermal and fluid dynamics behavior, making it suitable for applications prioritizing uniformity over high heat transfer rates.

Overall Comparison and Insights

When comparing the three patterns, it becomes evident that each design offers unique advantages and trade-offs. Pattern 1 strikes a balance between pressure stability, moderate heat transfer efficiency, and relatively uniform thermal behavior, making it a versatile choice for applications requiring a compromise between stability and performance. Pattern 2 stands out for its stability and consistency, with lower pressure fluctuations, uniform temperature distribution, and steady heat transfer characteristics. While it sacrifices some heat transfer efficiency, its predictable performance makes it ideal for scenarios where thermal uniformity and flow stability are prioritized. Pattern 3 , on the other hand, excels in convective heat transfer efficiency, achieving the highest Nusselt number. However, this comes at the cost of elevated temperatures and reduced pressure stability, which may lead to localized hotspots and uneven thermal performance. As such, Pattern 3 is best suited for applications demanding high heat transfer rates, where thermal uniformity and pressure stability are secondary concerns.

In conclusion, the summarized data from Tables 3, 4, and 5 provides a comprehensive view of how each pattern performs under varying conditions. By evaluating pressure, temperature, and Nusselt number, it is clear that the choice of pattern depends on the specific requirements of the application, whether prioritizing stability, efficiency, or thermal uniformity.

Table 3 Average of Pressure on inlet jet

Pattern 1	Pattern 2	Pattern 3
213371 [Pa]	192302 [Pa]	186990 [Pa]

Table 4 Area Average of Temperature on heater wall

Pattern 1	Pattern 2	Pattern 3
22.048 [°C]	22.226 [°C]	26.82 [°C]

Table 5 Area Average of Surface Nusselt Number on heater wall

Pattern 1	Pattern 2	Pattern 3
2.42394e^{06}	1.87839e^{06}	4.29601e^{06}

Figure 27 provides a 3D visualization of the geometry and highlights key measurement lines centerline, a line at 100 μm distance, and a line at the edge—that are critical for analyzing fluid flow and thermal behavior across the domain. The geometry features vertical posts or pillars arranged in a symmetrical and periodic pattern, which likely influence pressure, temperature, and velocity distributions. A red dashed line marks the centerline , representing the central axis of the domain and serving as a reference for symmetric flow conditions. A yellow dashed line at 100 μm from the centerline captures intermediate behavior, showing how flow properties transition from the center to the edges. Another yellow dashed line near the edge focuses on boundary effects, where turbulence and localized phenomena may significantly impact flow dynamics and heat transfer. Arrows (e.g., v) indicate the direction of fluid flow, emphasizing the role of computational fluid dynamics (CFD) simulations in studying these interactions.

These graphs present conclusions that the variation of the Nusselt number (Nu) , pressure drop (ΔP) , and other parameters depend significantly on the Reynolds number (Re) , volume flow rate (m^3/s) , and a porosity value of 0.9 . In all cases, the employment of a Pyrex substrate material leads to a noticeable variation in the Nusselt number and a reduction in the pressure drop (ΔP) compared to the baseline flow case without such material. This indicates that the choice of substrate material plays a crucial role in enhancing heat transfer efficiency while reducing flow resistance. As can be seen in the graphs, the Nusselt number increases with higher Reynolds numbers , reflecting improved convective heat transfer due to increased flow turbulence and fluid interaction with the heated surface. Simultaneously, the pressure drop decreases, suggesting that the Pyrex substrate mitigates flow resistance despite elevated flow rates. These findings underscore the importance of optimizing material selection and flow parameters to achieve a balance between enhanced heat transfer performance and minimized pressure losses, particularly in systems operating under varying Reynolds numbers and permeabilities.

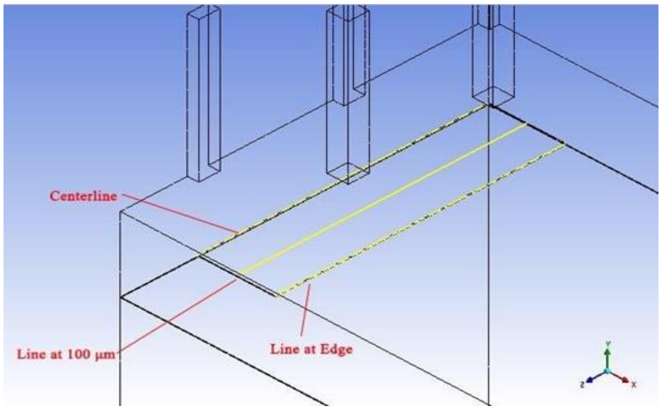

Figure 27: Lines of plots starting from center

Conclusion

This work presents a comprehensive numerical investigation aimed at enhancing heat transfer through jet impingement at a volume flow rate of 45, with varying results obtained for different Nusselt numbers. The study employed the finite volume method and the SIMPLE algorithm scheme using ANSYS FLUENT to simulate and analyze key parameters such as Nusselt number (Nu), pressure drop (ΔP), temperature distribution, and velocity profiles. The results demonstrate that these parameters gradually increase with respect to fluid flow velocity, highlighting the interplay between flow dynamics and thermal performance.

The findings reveal that both the pressure drop and Nusselt number for laminar flow increase rapidly with an increase in the Reynolds number , underscoring the significant influence of flow conditions on heat transfer efficiency and fluid resistance. The numerical study demonstrates the feasibility of achieving highly accurate predictions of temperature and heat flux distributions within the medium. This was accomplished by solving the Energy Equation model using the finite volume method, which facilitated steady-state simulations of natural convection heat transfer in a 3D channel. The coupling of pressure and velocities was achieved through the SIMPLE algorithm , ensuring robust and reliable results.

A primary objective of this study was to determine key parameters such as permeability (k), average Nusselt number (Nu) , and pressure drop for convective heat transfer in the given medium, alongside analyzing the temperature distribution. The results indicate that the average Nusselt number increases with Reynolds number and the ratio of the half-length of the heated copper plate to its diameter (R/d), but decreases with the ratio of the orifice plate length to its diameter (L/d). Furthermore, the pressure coefficient was found to be higher at lower values of r/d, while the mean velocities showed a strong correlation with the heat transfer coefficient.

An important observation from the study is that the Nusselt number remains nearly equal at edges 1 and 2, but significantly increases at edge 3, indicating localized enhancements in heat transfer near the periphery. This behavior highlights the influence of geometric design and boundary effects on thermal performance. Additionally, it was noted that the Nusselt number is a function of five non-dimensional parameters: Reynolds number (Re), Prandtl number (Pr), normalized distance along the z-axis (z/d), length-to-diameter ratio of the orifice plate (L/d), and radius-to-diameter ratio of the heated surface (R/d).

In summary, this numerical study provides valuable insights into optimizing heat transfer and fluid dynamics for cooling high-power mini-devices. While each geometric model exhibits unique characteristics and potential deficiencies, the analysis underscores the importance of balancing enhanced heat transfer with minimized pressure losses. These findings can guide future designs in applications requiring efficient thermal management, particularly in systems operating under varying flow and thermal conditions.

CRediT authorship contribution statement

Attiq Ur Rehman: Methodology, Conceptualization, Writing – original draft, Visualization, Writing – review & editing, **Hassaan Ahmad:** Writing – Review & Editing, Methodology, **Khawar Abbas:** Writing – review & editing, **Muhammad Shahid Farooq and Dong Yang:** Supervision, Project administration, Resources.

Declaration of competing interest

The authors declare that they have no known competing financial interests or personal relationships that could have appeared to influence the work reported in this paper.

Acknowledgment

We extend our sincere gratitude to our academic advisors and the technical team at Xi'an Jiaotong University, for their guidance and support in utilizing tools like ANSYS FLUENT, which were essential for this research. Special thanks to our colleagues and peers for their insightful discussions and feedback, which greatly enriched the study.

Data availability

Data will be made available on request.

Nomenclature

Symbols	
a	Specific surface area (fluid to solid contact) [m^2]
Nu	Nusselt Number
d_p	Spherical particle diameter, fluid to solid heat transfer coefficient [w. m^{-1}. K^{-1}]
k	Thermal conductivity [w. m^{-1}. K^{-1}
μ	dynamic viscosity [kg. m^{-1}. s$^{-1]}$
H	Height of the plate
C_p	Specific heat at constant pressure
ρ	density [kg. m^3]

REFERENCES

[1] P.-X. Jiang and X.-C. Lu, “Numerical simulation of fluid flow and convection heat transfer in sintered porous plate channels,” Int. J. Heat Mass Transf., vol. 49, no. 9, pp. 1685–1695, 2006, doi: https://doi.org/10.1016/j.ijheatmasstransfer.2005.10.026.

[2] O. D. Makinde, “On MHD boundary-layer flow and mass transfer past a vertical plate in a porous medium with constant heat flux,” Int. J. Numer. Methods Heat Fluid Flow, vol. 19, no. 3–4, pp. 546–554, 2009, doi: 10.1108/09615530910938434.

[3] I. A. Badruddin, Azeem, T. M. Yunus Khan, and M. A. Ali Baig, “Heat Transfer in Porous Media: A Mini Review,” Mater. Today Proc., vol. 24, pp. 1318–1321, 2020, doi: https://doi.org/10.1016/j.matpr.2020.04.447.

[4] K. M. Shirvan, M. Mamourian, S. Mirzakhanlari, R. Ellahi, and K. Vafai, “Numerical investigation and sensitivity analysis of effective parameters on combined heat transfer performance in a porous solar cavity receiver by response surface methodology,” Int. J. Heat Mass Transf., vol. 105, pp. 811–825, 2017, [Online]. Available: https://api.semanticscholar.org/CorpusID:125873374.

[5] U. K. Suma, M. Masum Billah, and A. R. Khan, “Optimization and sensitivity analysis of unsteady MHD mixed convective heat transfer in a lid-driven cavity containing a double-pipe circular cylinder using nanofluids,” Int. J. Thermofluids, vol. 27, p. 101197, 2025, doi: https://doi.org/10.1016/j.ijft.2025.101197.

[6] G. Q. Xu, Z. X. Jia, J. Wen, H. W. Deng, and Y. C. Fu, “Thermal-Conductivity Measurements of Aviation Kerosene RP-3 from (285 to 513) K at Sub- and Supercritical Pressures,” Int. J. Thermophys., vol. 36, no. 4, pp. 620–632, 2015, doi: 10.1007/s10765-015-1840-4.

[7] P. C. Barman, “A Study on Phase diagram of a binary mixture,” vol. 4, no. 3, pp. 3501–3504, 2017.